LUNDS UNIVERSITET

Construction of a ^{14}C bomb-pulse dating calibration curve relevant for man

Sonny Nilsson

September 13, 2018

Bachelor Diploma Work
Project duration: 15 Jan - 7 May 2018
Supervised by Kristina Stenström
Department of Physics - Division of Nuclear Physics

Abstract

Radiocarbon dating has great potential in medical applications. A consequence of the complex path of radiocarbon to humans through diet is that the radiocarbon content of samples from human subjects is not directly comparable with the atmosphere's. By considering the harvest seasons in Sweden and its surrounding countries, a new software was developed to further investigate if the accuracy of the dating could be improved for 60 and 17 Swedish blood serum samples from 1978 and 2005-2013, respectively. A substantial increase in accuracy was obtained for the older samples but on the other hand, there was a slight decrease in accuracy for the more recently taken samples.

Contents

Abbreviations

δ^{13}**C**	Relative deviation of the $^{13}C/^{12}C$ ratio of the sample compared to that of the standard material VPDB (Vienna Pee Dee Belemnite)
AMS	Accelerator mass spectrometry
C3	Calvin-Benson enzymatic pathway
C4	Hatch-Slack enzymatic pathway
CAM	Crassualacean Acid Metabolism
F^{14}C	Fraction modern carbon, dimensionless quantity.

1 Introduction

Atmospheric nuclear weapon testing during the middle of the last century caused the concentration of the radioactive carbon isotope ^{14}C to double in the northern hemisphere. This has given the opportunity to date organic materials with much higher accuracy than what would be otherwise possible with regular radiocarbon dating. Furthermore, dating human tissue is of great interest in, among other areas, medicine. Several papers previously published by the Biospheric and Anthropogenic Radioactivity Group (the BAR group) at the Division of Nuclear Physics at Lund University [1-3], has dated samples from humans (plaque and blood serum) with a software called Calibomb made by researchers at the Queen's University, Belfast, in the department Centre for Climate, the Environment and Chronology [4]. However, the ^{14}C concentration in human tissue is a consequence of the ^{14}C concentration in the subject's diet. On one hand, Calibomb is suited for dating organic materials which have similar ^{14}C concentration as the atmosphere, such as plants. On the other hand, for samples deviating from this rule, such as humans, the diet has to be considered.

For countries in northern Europe, the foodstuff is seasonal. Therefore, a program similar to Calibomb has been constructed to account for the effect of consuming stored food which will be referred to as Caliman. This paper aims to construct this program in a realistic manner and simultaneously improve the systematic accuracy of radiocarbon dating of samples from human subjects.

2 Theory

2.1 ^{14}C on Earth

2.1.1 Natural ^{14}C

When high-energetic charged particles such as protons, alpha particles and electrons from cosmic radiation collide with particles in the stratosphere, fragments in the form of free neutrons are frequently produced. These neutrons can react with nitrogen in the reaction $n+^{14}\mathrm{N}\rightarrow^{14}\mathrm{C}+p$. However, the total production in this reaction is not constant since there is a variance in the cosmic radiation flux. Additionally, the magnetic field of the earth slightly change direction and strength over time. Consequently, this makes the amount of cosmic radiation colliding with the atmosphere to fluctuate [5]. The ^{14}C produced is then oxidized to $^{14}CO_2$ which is then mixed with $^{12}CO_2$ and $^{13}CO_2$ in the atmosphere and hydrosphere. These isotopes are present in the atmosphere in the amount presented in Table 1 [6]. The ^{14}C can then be absorbed by the biosphere and therefore humans. The isotope ^{14}C is unstable and thus decays in these different reservoirs through β-decay. It has a half-life of 5730 ± 40 years [7].

Table 1: Approximate abundance of carbon isotopes in the atmosphere [6]

Isotope	Ratio (%)
^{12}C	98.89
^{13}C	1.11
^{14}C	10^{-10}

Since the abundance of ^{14}C and its half life are known it is possible to calculate the specific activity of ^{14}C with the formula

$$A = \frac{\ln(2)}{T_{1/2}} \cdot N_A \frac{m_{^{14}\mathrm{C}}}{M_{^{14}\mathrm{C}}} \Big/ m_C$$

where $T_{1/2}$ is the half life, N_A is the Avogadro's constant, $M_{^{14}\mathrm{C}}$ is the molar mass of ^{14}C , $m_{^{14}\mathrm{C}}$ is the total mass of ^{14}C isotopes and m_C is the total mass of carbon. The equation can be rewritten:

$$\begin{aligned} A &= \frac{\ln(2)}{T_{1/2}} \cdot N_A \frac{n_{^{14}\mathrm{C}} M_{^{14}\mathrm{C}}}{n_{\mathrm{C}} M_{\mathrm{C}}} \Big/ M_{^{14}\mathrm{C}} \\ &= \frac{\ln(2)}{T_{1/2}} \cdot N_A \frac{n_{^{14}\mathrm{C}}}{n_{\mathrm{C}}} \frac{1}{M_{\mathrm{C}}} \end{aligned}$$

Compared to the measured atmospheric activity of approximately 226 Bq/kg C [8], the calculation gives $A = 192$ Bq/kg C which is within the uncertainty of the given abundance of ^{14}C using the value given in Table 1.

2.1.2 Anthropogenic ^{14}C

After world war two the superpowers of the world tested nuclear bombs in large scales, and atmospheric testing was the most common in the beginning. However, when the Partial Nuclear Test Ban Treaty was approved by most countries, atmospheric nuclear bomb tests were stopped entirely by USSR and USA. Although France and China continued with these tests after 1963, their combined number of bombs detonated was less than 14% of the total number [9].

Under the process of fission (and fusion) free neutrons are released. These neutrons can react with the nitrogen rich air. In this process ^{14}C is formed, which is then oxidized to carbon dioxide.

One of the consequences of the large scale nuclear bomb tests in the atmosphere was that the ^{14}C concentration in the northern hemisphere doubled [10], see Figure 1. From the peak in 1963, the ^{14}C concentration has decreased approximately exponentially. This decrease can be utilized to radiocarbon date organic materials. Today, the concentration is converging to the natural level which makes dating of materials from the last decade, using the bomb-pulse method, less accurate.

On one hand, in equilibrium the ^{14}C distribution in the atmosphere and the different reservoirs equal after considering isotope fractionation (see Section 2.3). On the other hand, when in non-equilibrium (which is always the case) the distribution of ^{14}C varies. In the atmosphere, the ^{14}C concentration is approximately equal in the northern and southern hemisphere, respectively. However, according to Hua and Barbetti [11] the spatial distribution of bomb ^{14}C during the bomb peak was dependent on atmospheric circulation rather than simply the latitude. This circulation further creates three different zones in the northern hemisphere with distinctive atmospheric concentrations of ^{14}C . The concentration of ^{14}C in atmospheric CO_2 (in fraction modern carbon, see Section 2.4) in Europe can be seen in Figure 1.

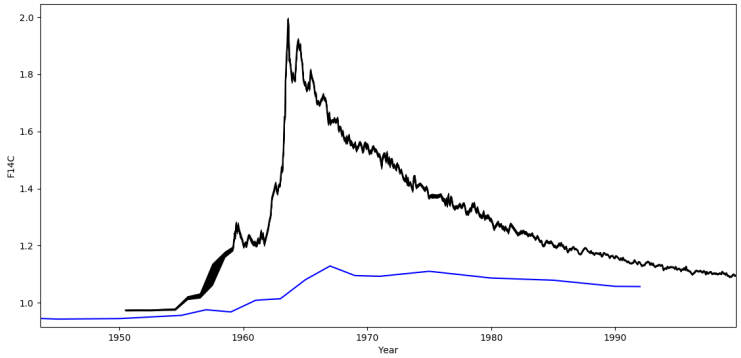

Figure 1: The upper black line is the ^{14}C concentration in atmospheric CO_2 in the northern hemisphere and the lower blue line is the ^{14}C concentration in marine species in the Barents Sea. The atmospheric data set was measured in Jungfraujoch and Schauinsland, Switzerland/Germany [10] and marine data set was measured in the Barents Sea [17].

Another anthropogenic source of ^{14}C is nuclear power plants. Due to the presence of one or more of the isotopes ^{14}N, ^{17}O and ^{13}C in the fuel, core structural materials and reactor coolant, ^{14}C is produced in neutron-induced nuclear reactions. Most of the produced ^{14}C end up as solid waste [12]. The three most common reactions producing ^{14}C can be seen in table 2. Furthermore, some of the ^{14}C is released in the atmosphere, see Table 3.

Table 2: Reaction, cross-section with thermal neutrons and natural abundance for most common isotopes that produce ^{14}C in nuclear power plants [12].

Reaction	Thermal cross-section (barns)	Natural abundance(%) of parent isotope
$^{14}N(n, p)^{14}C$	1.81	99.6349
$^{13}C(n, \gamma)^{14}C$	0.0009	1.103
$^{17}O(n, \alpha)^{14}C$	0.235	0.0383

In table 3 the total production of ^{14}C from the three largest sources is presented.

Table 3: Production rates of different sources [13]

Natural production	1.4×10^{15} Bq/year
Nuclear plants release	2.9×10^{14} Bq/year
Nuclear bomb total release	2.2×10^{17} Bq

2.2 Distrubution of ^{14}C

2.2.1 Ocean

The ocean works as a reservoir for the ^{14}C in the atmosphere, thereby decreasing the ^{14}C content in the atmosphere. Generally, the diffusion of a material within a medium, or between two media, is not instant. Consequently, diffusion causes the top layer of the ocean to have lower ^{14}C concentration than the atmosphere. A box diffusion model has been made [14] that differentiate the ocean into two layers - mixed layer and deep sea. In this model the content of ^{14}C varies with the oceans depth which further can affect the ^{14}C concentration in different marine species. Marine data sets of ^{14}C exist, but the content fluctuates regionally [15-16]. Consequently, the fluctuating ^{14}C concentration could potentially affect the ^{14}C concentration in the rest of the marine species, such as fish, in these regions.

In Figure 1 the lower blue line represents an example of a marine ^{14}C concentration data set. The data was extracted from cod otoliths from the Barents Sea [17].

2.2.2 Biosphere

In addition to the ocean, the biosphere also works as a reservoir that absorbs ^{14}C in the form of CO_2. It is reasonable to think that the ^{14}C content in the biosphere would be the same as atmosphere's. However, this is only approximately (although slightly different due to isotope fractionation) true for terrestrial plants. For marine plants and plankton, the ^{14}C content can be comparable with the ocean's, but higher up in the food chain it becomes more complicated. Fish typically migrate around in the ocean which has a fluctuating ^{14}C value.

The transportation of carbon to humans typically follows the path illustrated in Figure 2. In countries with a harvest season, crops should be largely produced during this period. Crops use photo synthesis to grow. Therefore the growth rate of a plant should reflect the plant's carbon absorption from the atmosphere, and thus the ^{14}C absorption. Consequently, the ^{14}C concentration in a plant can after normalization be compared to the atmospheric ^{14}C concentration (see Figure 1) under the growth period. Furthermore, the consumed crops during the rest of the year should, excluding imported crops, originate from former harvest period(s).

Livestock are typically fed with crops or products made from crops. Since the carbon absorption of these animals originates from the diet, the diet should reflect their ^{14}C concentration. The generic biokinetic model used by the International Commission on Radiological Protection approximates the carbon to be uniformly distributed in the body with a half-life (comparable with half-life of radioactive isotopes) of 40 days [18]. Another study conducted by Tieszen et al. [19] examined the speed in which carbon in rat tissues gets replaced by carbon derived from the subject's diet, where an exponentially decreasing model was used. The half-life of the tissues examined in the study ranged from approximately one week (liver) to 6 weeks (hair). On the other hand, different tissues in animals generally have different replacement rates.

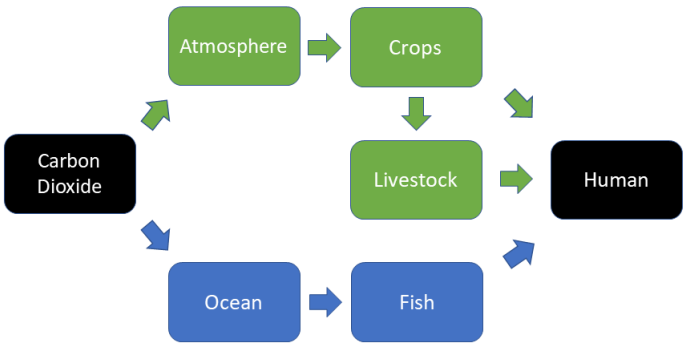

Figure 2: Illustration of the carbon transport to humans.

2.2.3 Local variations of ^{14}C

Combustion of fossil fuels increases the CO_2 content in the atmosphere. However, since the age of fossil fuels is much larger than the half-life of ^{14}C, these fuels contain almost no ^{14}C. Consequently, the ^{14}C concentration decreases globally and this is called the Suess effect. More importantly to consider is the local effect in, and close to, urban areas where there are large amounts of combusted CO_2. The ^{14}C /C ratio around strong CO_2 emitting regions is lowered [21] which can further decrease the ^{14}C concentration of the nearby vegetation. Additionally, since the use of fossil fuels is increased during the winter and decreased during summer, the local Suess effect fluctuate seasonally [22].

Opposite to strong CO_2 emitting sources, the anthropogenic ^{14}C from nuclear power plants causes an increase in ^{14}C locally. Consequently, the local vegetation of these plants could have an increased ^{14}C concentration.

2.3 Isotope Fractionation

Isotopes are atoms of the same element, thus having the same proton and electron number. However, isotopes have a different neutron number, making the mass of different isotopes to differ.

As a result of isotopes having variation in mass, they have slightly different physical and chemical properties [24]. These properties can result in that the proportions of isotopes become different between two materials in chemical equilibrium. For a chemical reaction out of equilibrium, such as photosynthesis, forward and backward reaction rates are not identical. Due to the chemical bond in molecules being stronger for larger masses, the reaction rates are therefore dependent on the ratio of masses between isotopes, thus creating different isotope ratios between the reactants and products. This process is called kinetic fractionation. Additionally, chemical and physical processes that discriminate certain isotopes over others in equilibrium are called equilibrium fractionation.

Since the relative ratios of certain isotopes differ in different materials, they can be compared using the notation δ. To compare, a standardized constant, from the international standard Pee Dee Belemnite

(PDB), is set to $\left(\frac{^{13}C}{^{12}C}\right)_{standard} = 0.0112372$ [23]. $\delta^{13}C$ is then calculated according to:

$$\delta^{13}C = \frac{\left(\frac{^{13}C}{^{12}C}\right)_{sample} - \left(\frac{^{13}C}{^{12}C}\right)_{standard}}{\left(\frac{^{13}C}{^{12}C}\right)_{standard}}.$$

Worth noting is that δ^{13}C is linearly increasing with $\left(\frac{^{13}C}{^{12}C}\right)_{sample}$. Typical values of δ^{13}C relative to PDB standard can be found in Table 4.

Table 4: δ^{13}C for different materials [25]

Material	δ^{13}**C : Mean (Range) [‰]**
Marine carbonates	0 (-4 to +4)
Atmospheric CO_2	-9 (-11 to -6)
Grains, seeds, maize, millet	-10 (-13 to -7)
Marine organisms	-15 (-19 to -11)
Bone collagen, wood cellulose	-20 (-24 to -18)
Grains (wheat, oats, rice, etc)	-23 (-27 to -19)
Recent wood, charcoal	-25 (-30 to -20)
Tree leaves, wheat, straw	-27 (-32 to -22)

In the case of plants, where photosynthesis is essential for the growth, both equilibrium- and kinetic fractionation is present [26]. Furthermore, plants can be clustered into three different groups based on their general values of δ^{13}C : C3, C4 and Crassualacean Acid Metabolism (CAM). Included in Table 5 are typical plants divided into the three groups.

Table 5: Photosynthetic pathways for some materials [27]

Photosynthesis	**Examples**
C3	flowering plants, trees, most temperate zone grasses, wheat, potatoes
C4	corn, sugar cane
CAM	tropical plants, pineapple

Typical values of δ^{13}C in C3 plants is -27‰ and for C4 plants -13‰. In contrast, CAM plant's δ^{13}C depends more on environmental factors, such as the light setting [28].

Since the human value of δ^{13}C is almost equal to the corresponding value of the consumed food after accounting for carbon isotope fractionation [20], isotope analysis can be used to determine the diet of a subject. However, δ^{13}C values generally overlap between different species of plants and animals. Marine foodstuffs such as fish tend to have overlapping δ^{13}C to C4 plants. Therefore, another parameter is required to differentiate distinct plants and animals based on carbon isotope fractionation alone [29]. δ^{15}N, which represents the abundance of ^{15}N and ^{14}N similarly to δ^{13}C , can be used for this since food from the marine environment generally has larger values than terrestrial ones [20]. δ^{15}N can in combination with δ^{13}C be used to create an isotopic trophic level diagram. With foodstuff having known regions in the diagram, cluster analysis can be used to reveal information about the diet, such as fish consumption, of the subjects.

2.4 Fraction Modern Carbon

The term Fraction modern carbon ($F^{14}C$) was established by Paula J Reimer et al. [30] to standardize the way ^{14}C concentration is written.

Let A_S be the specific activity [Bq/kg C] from ^{14}C in a sample. However, due to isotope fractionation of different biotic materials, A_S can not be used directly. A new factor, F, is introduced that, when multiplied with the activity, defines a new activity, A_{SN}, which normalizes the activity to a standard material (piece of wood with $\delta^{13}C$=25‰) :

$$A_{SN} = A_S \cdot F_{14/12}$$

where the factor F is called the fractionation factor. It compares the ratio of one carbon isotope to another carbon isotope between a sample and the piece of wood. The fractionation factor comparing carbon 12 and 13 is for example defined as:

$$F_{13/12} = \frac{\left(\frac{^{13}C}{^{12}C}\right)_{[\delta^{13}C=-25]}}{\left(\frac{^{13}C}{^{12}C}\right)_S}$$

where the numerator and denominator is the fraction of $\frac{^{13}C}{^{12}C}$ in the comparison material and sample, respectively. According to Stuiver and Robinson [32], $F_{14/12}$ can further be written:

$$F_{14/12} \approx F_{13/12}^2$$

which consequently gives the normalized activity:

$$A_{SN} \approx A_S\left(\frac{1-\frac{25}{1000}}{1+\frac{\delta^{13}C}{1000}}\right)^2$$

With the normalized activity it is possible to compare the ^{14}C content of two materials. For example, the calibration data set used in figure 1 is normalized to −25‰. To further compare the calibration data set to a given sample, the specific activity also has to be normalized to −25‰. Additionally, the specific activity decreases over time. To obtain a value which is time independent, the absolute radiocarbon standard, A_{abs}, is used which is defined as:

$$A_{abs} = 226 \text{ Bq}$$

A_{abs} can also be written as:

$$A_{abs} = A_{1950[-25]} e^{\lambda_C (y-1950)}$$

where $\lambda_C = 1/8267 \text{yr}^{-1}$ and y is the year of measurement and $A_{1950[-25]}$ is the hypothetical specific activity in year 1950's atmosphere normalized to the piece of wood, decayed to present. The previous reference specific activity was obtained from oxalic acid made from crop of sugar beet harvested 1955. Since the ^{14}C concentration has increased since 1950, $A_{1950[-25]}$ is defined as 95%, the correction factor, of the normalized specific activity of the oxalic acid. However, this reference sample is not available anymore but there exist several other reference samples. One of those is called OxII (SRM 4990 C) where $\delta^{13}C_{OxII} = -17.8$‰ and the correction factor instead becomes 0.7459. The final transformation is:

$$A_{1950[-25]} = 0.7459 A_{OxII} F_{14/12} = 0.7459 A_{OxII}\left(\frac{1-\frac{25}{1000}}{1-\frac{17.8}{1000}}\right)^2$$

Fraction Modern Carbon is defined

$$\mathrm{F}^{14}\mathrm{C} = \frac{A_{SN}}{A_{1950[-25]}}$$

and is the modern quantity to describe the ^{14}C concentration in a sample. This unit is independent of time.

2.5 Radiocarbon dating

One radiocarbon dating method of a sample is described in Stuiver and Pearson [31]. In this method, a data set of representative atmospheric ^{14}C concentration values, called calibration data set, is measured or given. For some i, let the statistical uncertainty of one sigma $\sigma_{i,cali}$, for the calibration data, $X_{i,cali}$, be given for each time frame (the time between two data points is varying). Since the quantity $\mathrm{F}^{14}\mathrm{C}$ is constant with time, the sample uncertainty of one sigma, σ_{sample}, and the sample data point, X_{sample}, will also be constant with time. When X_{sample}=$X_{i,cali}$ for some i the date of the sample can be directly read from the intersection point. To evaluate the uncertainty, consider the function $f = X_{sample} - X_{i,cali}$. Since X_{sample} and $X_{i,cali}$ are independent of each other, the uncertainty of f can be written:

$$\sigma_{i,f} = \sqrt{\left(\frac{\partial f}{\partial X_{i,cali}}\right)^2 \sigma_{i,cali}^2 + \left(\frac{\partial f}{\partial X_{sample}}\right)^2 \sigma_{sample}^2} = \sqrt{\sigma_{i,cali}^2 + \sigma_{sample}^2}$$

To evaluate which range of dates there is $\pm 1\sigma$ chance for the sample to be in one checks where $\pm\sigma_f$ intersects f. Since X_{sample} is constant, this is equivalent to check where $X_{sample} \pm \sigma_{i,f}$ intersects $X_{i,cali}$. The uncertainty of X_f has a gaussian shape and thus a probability distribution can be evaluated which is defined as:

$$g = \frac{1}{\sigma_{i,f}\sqrt{2\pi}} \exp(-1/2(f/\sigma_{i,f})^2)$$

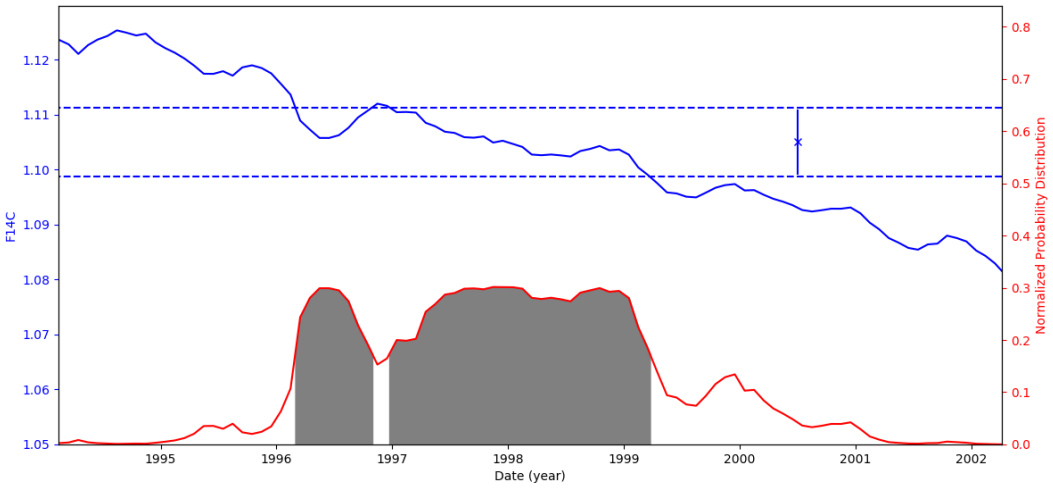

Figure 3: Output from dating software for one sample (x mark). The filled, blue line (located topmost) is the centerline of the calibration curve. The dotted line is $X_{sample} \pm \sigma_{i,f}$. The filled, red line (located at bottom) is the probability distribution and the shaded areas are the regions the sample is at $\pm\sigma_{i,f}$ probability

Note that in Figure 3, the dotted line is constant and close to the uncertainty in the sample in this region since the uncertainties in the calibration curve is constant and small compared to sample uncertainty.

Typically one to three boundaries will be evident within one sigma.

Several papers [1-3] that used Calibomb (which uses similar algorithm as described above) to date samples, used the mean of the first boundary to the last boundary, and the uncertainty as the difference between these two boundaries divided by two. This does not give the whole picture as the probability distribution is not a gaussian and there may be several regions in the said boundaries not included in $\pm\sigma_{i,f}$. However, since these regions are typically small and one value that can easily be compared to the sampling date is desired, this comparison is representative of the shaded region in Figure 3.

2.6 Connection between Diet and ^{14}C Values in Humans

The carbon content of humans has its origin from the foodstuff consumed. Consequently, the ratio of the carbon isotopes in humans reflects the origin of the foodstuff. However, the diet of individuals vary and thus the ^{14}C concentration in humans also vary [33]. For example; eating large quantities of fish, which generally contain a smaller concentration of ^{14}C (see Figure 1), reduces the consumer's ^{14}C concentration as well [34] .

According to Nydal et al. [35] the time between photosynthesis of vegetational foods and their consumption makes the consumer seem correspondingly older. For example eating only canned food dated 6 months will create an additional 6 month time lag in the consumers ^{14}C concentrations, while in contrast eating only fresh foods will not.

Further Nydal et al. state that the residence time of the carbon in the constituents of human tissues varies. Broecker et al. [36] compared the ^{14}C concentration of the atmosphere and different tissues in the human body. They found a lag corresponding to 1 and 1.8 years for blood and lung tissue, respectively. Further they found that blood has a maximum of 6 months lag compared to the food ingested. However, for blood serum the residence time of carbon is shortened to just a couple of days [37]. Consequently, blood serum reflects the ^{14}C concentration of the diet.

2.7 Medical Applications of Carbon Dating

The principle of radiocarbon dating can be used medically. In the case of the disease atherosclerosis, fat is accumulated inside the intima of the arterial walls, producing a deposit called plaque (see Figure 4). Initially the interface of the first and second layer - the intima and media - starts to grow. The inside of the intima then starts to grow into a core and then swells up (see Figure 4). Finally the media cells starts to produce the cap to prevent blood from coming in contact with the fat deposits between the walls. Consequently, rupture of the cap leads to thrombosis which may cause heart attack and stroke. Estimates made by Beckman et al. [38] concluded that between 60000 and 100000 Americans die each year from the disease.

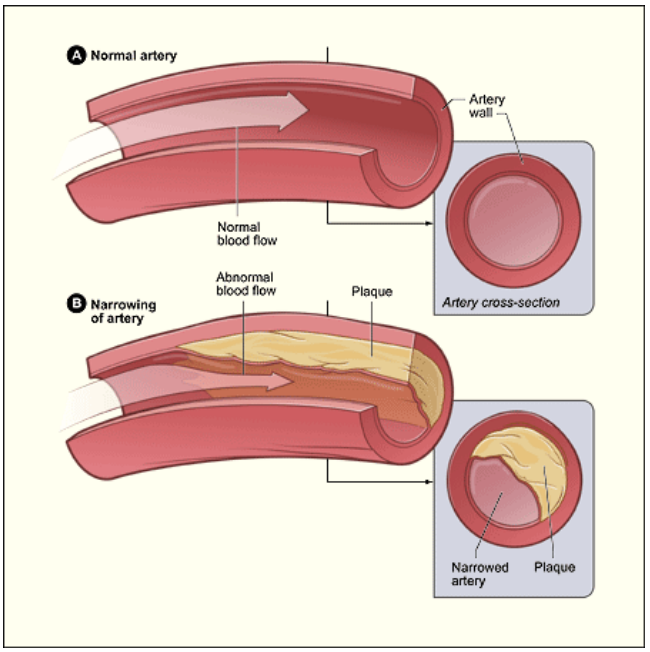

Figure 4: Illustration of plaque accumulating in the arterial walls.

In three independent studies the formation of the three different regions of the plaque has been measured, which when subtracted by the date of surgery gave the age of the regions. The age and the uncertainties obtained by the Calibomb software are given in Table 6. This confirms the order in which the three regions are formed.

Table 6: Age of the three different of the three regions in three separate studies [1-3]. These studies used clean air atmospheric calibration data as reference (see Figure 1). SEM is the standard error of the mean.

Study	A Swedish patients $N = 10$ Operation year: 2007-2009 Isabel Gonçalves et al	B Portuguese patients $N = 20$ Operation year: 2000-2001 Andersson Georgiadou et al	C Swedish patients $N = 16$ Operation year: 2005-2011 Eriksson Stenström et al
Plaque region	Mean age (y) $\pm 1\sigma$ / SEM	Mean age (y) $\pm 1\sigma$ / SEM	Mean age (y) $\pm 1\sigma$ / SEM
Cap	6.4 ± 5.5/1.4	5.5 ± 2.6/0.6	8.1 ± 4.4/1.1
Core	9.8 ± 4.5/1.4	7.8 ± 3.7/0.8	9.2 ± 5.5/1.4
Interface to media	12.4 ± 3.3/1.0	9.7 ± 2.4/0.5	11.6 ± 3.9/1.0

3 Materials and Methods

3.1 Subjects and Samples

16 of the blood serum samples were collected from the Swedish plaque patients of study C (Table 4) at the time of surgery (2005-2011) at Skåne University Hospital, Malmö, Sweden. The samples were kept in a freezer at -80 °C prior to being sent to the Division of Nuclear Physics at Lund University.

The other blood serum samples (20 μl each) were obtained from the Malmö Biobank from 1978 and kept in a freezer at -25 °C until analysis. All subjects were residents of Malmö, Sweden at the time of sampling. Before sample preparation, the samples were thawed for 2 h [27].

To measure the ^{14}C /^{12}C ratio of the samples, thus measuring the F^{14}C value, they were first graphitizied and then the graphite was run through a Single Stage Accelerator Mass Spectrometer (SSAMS). The data sets used are attached in the appendix (Tables 10 and 11).

3.2 The Graphitization Process

Pure carbon is a necessarily to analyze the isotope ratios in the SSAMS, thus a graphitization process is needed. This process was very similar for the two sample sets and the graphitization process described in great detail in Genberg et al. [39], but will be briefly depicted here. A picture of the apparatus is can be seen in Figure 5. Before the process, the samples were dried in a preheated oven at 80 °C for 1 h while being placed in glass tubes covered with aluminum foil. The samples were then mixed with CuO in a quartz glass tube which is evacuated using a vacuum system. They were then combusted to CO_2 and other gases. To remove the other gases, except CO_2, the CO_2 was condensed in the combustion quartz tube by inserting the tube into liquid nitrogen (T=-196 °C). The frozen CO_2 remained in the tube while the vacuum system was used to remove the remaining gases. Afterwards, the CO_2 was transported to a reactor containing a quartz tube with a small amount of iron catalyst. After measuring the pressure in the reactor with a calibrated pressure sensor attached to the reactor, the CO_2 was frozen again and H_2 were added corresponding to three times the pressure of CO_2. When these gases were heated to 600 °C, graphite was formed on the catalyst. The graphite was then crushed into a fine powder and put into capsules. To not be contaminated, the capsules were stored in an inert gas (Ar) until they were put into the SSAMS. Primary standards (OxI), secondary standards (IAEA-C6 and IAEA-C7) and blanks were graphitized using the same procedure as the samples.

Figure 5: Picture of the conventional graphitization apparatus. Picture taken from: E Andersson Georgiadou: Exploring the possibilities of ^{14}C bomb-pulse dating of human tissue samples. Doctoral dissertation. Lund University, 2014.

3.3 Accelerator Mass Spectrometry

In Lund, the AMS used for the ^{14}C method is located in Geocentrum and is single staged (SSAMS), see Figure 6. When the sample wheel is put at the start of the system the air in the vacuum tubes is pumped out. Close to the sample wheel (1) cesium is placed which is then heated in an oven, evaporating to a gas. Next to the graphite sample an ionizer is located, in the geometrical form of a bowl with a hole in it. When the cesium gas is coming in contact with the ionizer, the cesium becomes ionized into positive ions through thermal ionization. An electrostatic field with the electric potential energy Vq is then applied in the direction from the disc to the sample, which causes the ions to accelerate towards the sample. The collisions cause some graphite atoms to gain one electron. The negative charged graphite ions are then accelerated in the opposite direction as the cesium ions. Consequently, a ion beam is created made of $^{12}C^-$, $^{13}C^-$, $^{14}C^-$ and some negatively single charged molecules such as $^{13}CH^-$. To change between the two ion sources (1) an electrostatic analyzer (ESA) is used (2). The components are two bending metal plates with radius r which are charged q_{plate} and $-q_{plate}$ with the spacing d. For a particle with charge q and velocity v to stay at constant radius r, thus constant potential, the centrifugal force, F_c, should be equal to the electrostatic force, F_E.

$$\vec{F_c} = \vec{F_E} \Rightarrow m\frac{v^2}{r}\hat{r} = qE\hat{r}$$
$$\Rightarrow \frac{2T}{r} = q\frac{\Delta U}{d} \Rightarrow \Delta U = -\frac{2Td}{re}$$

where T is the kinetic energy ($= Vq$). Consequently, by monitoring ΔU it is possible to choose which particles with specific ratios $\frac{T}{q}$ that passes. After the electrostatic analyzer, the particles go through an orthogonal magnetic field (3) relative to the beam path. The equation becomes:

$$F_c = F_B \Rightarrow m\frac{v^2}{R}\hat{R} = q\vec{v} \times \vec{B} \Rightarrow \quad \frac{B^2R^2}{2} = \frac{mv}{q} = \frac{2mT}{q^2}$$

where the quantity $\frac{B^2R^2}{2}$ is typically referred to as a magnet's bigness.

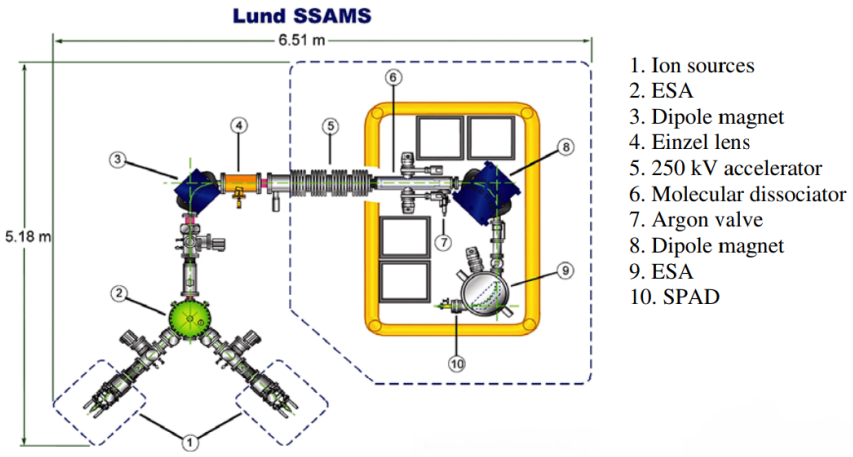

Figure 6: Illustration of the SSAMS located in Lund. Adapted from [39]

Since this formula is mass dependent only one of the isotopes $^{12}C^-$, $^{13}C^-$ or $^{14}C^-$ can get through this filter. Since the flow of the beam can change with time it is desirable to continuously detect all three isotopes simultaneously. Since this is not possible, ^{12}C is measured for 300 μs, ^{13}C for 900 μs and ^{14}C for the rest of the time every $\frac{1}{10}$ s. Since changing voltage over an coil does not instantly change the current through it, which the magnetic field is proportional to, the magnetic field lags behind the voltage inducing it if changed. This effect is referred to as hysteresis. To change which isotope that passes through the dipole at a fast rate, the kinetic energy is instead controlled through an electric field.

^{14}C shares approximately the same mass with common molecules such as ^{13}CH and $^{12}CH_2$. Therefore the isotopes are accelerated through an electric field (5) and collided with a noble gas (6) called molecular dissociator or gas-stripper. Since the acceleration in the electric field converges the beam, it is first focused by an Einzel lens (4), where the E-field of the accelerator is put after the focal point of the Einzel lens, making the beam divergent. Consequently, after the collision with the gas, the molecules are dissociated into their elemental components while the isotopes and some molecules become ionized into positive ions. The beam continues through another dipole magnet (8). Here, $^{12}C^+$ and $^{13}C^+$ are captured in Faraday cups. Since the intensity of the $^{14}C^+$ beam are 10 orders of magnitude smaller than the $^{13}C^+$ one, another ESA (9) is used on the beam. Lastly, an post-accelerator deflector (10) is attached to further keep other isotopes than ^{14}C from the detector.

3.4 Construction of Calibration Program

To compare the results of this paper and other papers, a reference program was written to analyze blood serum data which was constructed upon the same principles as described in (Stuiver and Pearson) [41]. In addition another modified version of this program was written which I will refer to as Caliman.

Due to updates where the uncertainty is handled differently, the official Calibomb produces dates slightly different than my reference program (no more than 3 months). The calibration data set used was taken in Jungfraujoch and Schauinsland [10] [42].

Since plants absorb CO_2 during their whole respectively growth period, different parts of plants have certain time lag behind the atmospheric carbon concentration. To simplify this complex process, Calibomb has an smoothing option that uses simple moving average defined as:

$$X_{i,cali} = \frac{1}{n} \sum_{n} X_{i-n,cali}$$

where n is the number of samples within the time threshold. I also implemented this in Caliman under the harvest season.

The motivation behind building a separate calibration program was to partly have an automated comparison process, and partly to becoming certain the same foundation is used in Caliman. Caliman was made to take into account the time between harvest and consumption of the plants. It is possible to build a complex model which considers the harvest periods for each crop, the gross import of each crop, meat and forage. However, according to a report by Jordbruksverket [43], Sweden did under 2016 import 59% of its total imported foodstuff and agricultural goods from Norway, Germany, Denmark and Netherlands, all of which have the same harvest seasons as Sweden. Furthermore, 80% is imported from Europe which is heavily weighted to the central to northern countries. Although some of the foodstuff and agricultural goods are exported again, Sweden also produces these goods. Therefore, a rough approximation can be made that all of our foodstuff is produced during the same harvest period as in Sweden. It also has to be accounted for that crops grow during the whole growing season. The smoothing method used here will assume that the crops grow between April to October and each successive month will be the moving average of all the previous. So the month April will not be smoothed while the ^{14}C concentration in May will be the average of April and May. The assumptions made in mind producing this program are:

- All plants grow at constant speed under the growing season (therefore simple moving average is used).
- Outside of the growing season, no newly grown food is introduced in the system.
- The consumption of stored food during harvest period decreases linearly. On the first day, only stored food is consumed and on the last day, only food harvested that year is consumed.

Consequently, a data point in the harvest season gets replaced according to:

$$X_{i,new} = (1 - t)X_{last} + \frac{t}{n}\sum_{n} X_{i-n,cali}$$

where X_{last} is the last calibration data point in the prior harvest season and t goes from [0, 1] during the harvest season. The same procedure is otherwise done as my reference program, see Figure 7.

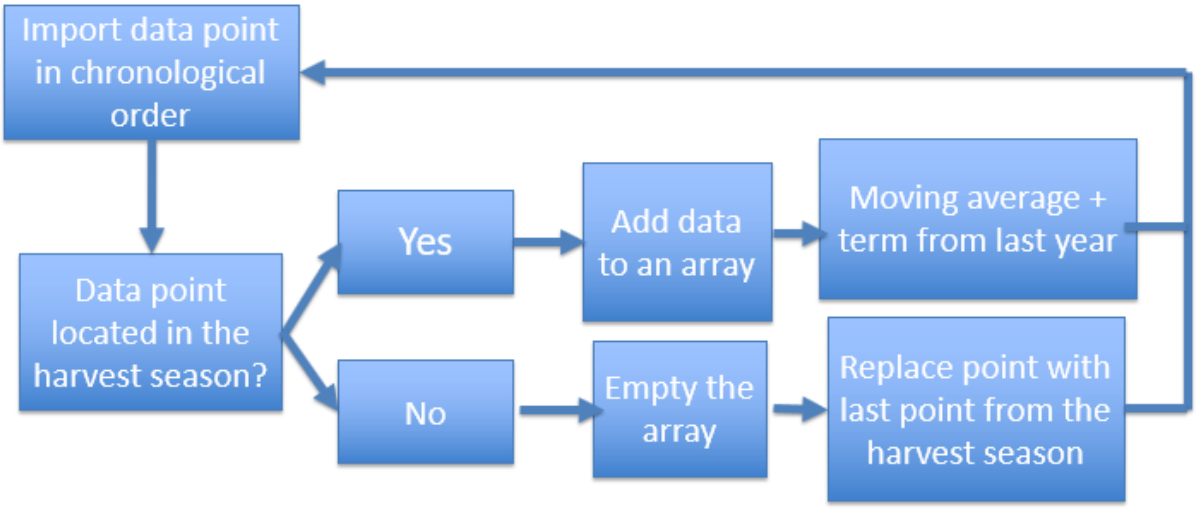

Figure 7: Simplified procedure of the calibration curve in the Caliman program

To compare the output of Caliman to the reference program, the squared error (SE) is used which is defined as:

$$SE = \sum_n f_n^2.$$

From this, root mean squared error (RMSE) can be calculated:

$$RMSE = \sqrt{\frac{SE}{n}}.$$

4 Result and Discussion

4.1 Comparison of reference program and Caliman

In the process of applying the Caliman program, Figures 8 and 9 were obtained. In Tables 10 and 11 the $F^{14}C$ values are presented for the samples. Since both the sample and calibration data sets are constructed by discrete data points, a linear approximation was made to find the ^{14}C concentration for the two calibration curves. The RMSE is presented in Table 7.

Table 7: RMSE for the samples from 1978 and 2005-2011.

	RMSE Reference program	RMSE Caliman	RMSE Ratio (Reference/Caliman)
1978	3.440E-3	1.756E-3	1.96
2005-2011	1.521E-3	1.750E-3	0.87

For the data set from 1978, the ratio of the RMSE between the programs indicates Caliman to have more similar $F^{14}C$ values compared to the sample data than my reference program. However, the data set was taken under a short interval (1978) with many samples (N=60) and therefore it is difficult to determine the predictive power of the model for other time spans. The sample data taken in the early 2000s have a similar problem, however with a larger time span (2005-2011) and smaller sample size (N=16) instead. For this data set, the ratio is instead 0.8.

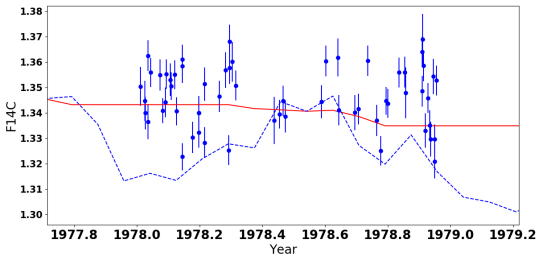

Figure 8: $F^{14}C$ values of the 1978 data samples and the calibration curves of Caliman (full, red line) and my reference program (dotted, blue line).

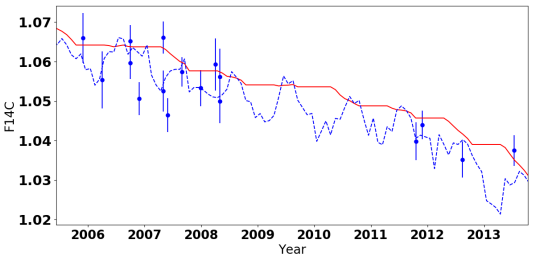

Figure 9: $F^{14}C$ values of the (2005-2011) data samples and the calibration curves of Caliman (full, red line) and my reference program (dotted, blue line).

In Tables 12 and 13 the predicted dates and their statistical uncertainty of 1 σ are calculated. This value is then subtracted from the operation year which is referred to as ΔT_R and ΔT_C, obtained from the reference program and Caliman, respectively. The average of $\Delta T \pm 1$ sigma is summarized in Table 8.

Table 8: Average age difference of samples predicted by the reference program (ΔT_R) and Caliman (ΔT_C) for the samples from 1978 and 2005-2011.

	ΔT_R (yr)	ΔT_C (yr)
1978	-1.22 ± 0.75	-0.47 ± 0.86
2005-2011	-0.15 ± 1.14	1.43 ± 1.50

The Caliman seems to date the samples approximately a year older than the reference program and with slightly larger average standard deviation.

Close inspection of Figures 8 and 9 shows that the (2005-2011) data set is above the calibration curves while in the 1978 data set they tend to be below (which the ΔT_R and ΔT_C also reveal). With current data it is only possible to speculate about the origin of this effect. One explanation of the different $F^{14}C$ distributions around the calibration curves is that there is some factor that is not accounted for. The sample type analyzed is the same, and time is already taken into account. However, the diet could be quite different for the subjects in 1978 compared to those in 2005-2011.

One of the largest factors influencing the carbon concentration in humans is consumption of fish since the $F^{14}C$ value in the ocean is notably lower than in the atmosphere (see Figure 1). According to Jordbruksverket [43] the consumption of fish was at a minimum around 1980, with the average consumption being approximately 1.8% of total energy intake. The number increases to 2.7% in 2010. Could this notably affect the ^{14}C concentration in the samples? Assume that the average $F^{14}C$ in fish in 1978 and 2010 follows the marine data set from the Barents Sea (see Figure 1). In 1978 the ^{14}C concentration was $F^{14}C \approx 1.1$. No data is available from 2005-2011 but assume $F^{14}C \approx 1$. The linear model used by Georgiadou and Stenström [44] can be used,

$$F^{14}C_{tot} = F^{14}C_{marine} X_{marine} + F^{14}C_{terrestrial}(1 - X_{marine}),$$

where X_{marine} is the proportion of marine food consumed. This effect causes the $F^{14}C$ value to be, on average, reduced by 0.01 in 1978 and close to 0 for 2005-2011. The average distance in squares when including consumption of fish can be seen in Table 9.

Table 9: RMSE for the samples, adjusted for fish consumption, from 1978 and 2005-2011.

	RMSE Reference program	RMSE Caliman	RMSE Ratio (Reference/Caliman)
1978	3.882E-3	2.070E-3	1.88
2005-2011	1.521E-3	1.854E-3	0.82

Consequently, Caliman got slightly worse (in terms of the factor difference) when considering consumption of fish in the calibration curve.

It is worth mentioning that the subjects of the 2005-2011 data had symptoms from atherosclerosis and were hospitalized before the samples were taken. On the contrary, the other subjects from 1978 had no symptoms of the disease and were not hospitalized. Speculatively, the medicine or for example nutrient solution could have been consumed the days before surgery, thus maybe having some impact on the ^{14}C content in the blood for the 2005-2011 samples.

Another explanation for the different distributions is that some organic compound could have been mixed into the blood serum samples taken 1978 or the ones taken 2005-2011.

4.2 Finding seasonal change

In the paper published by Georgiadou et al. [27] a graph with the difference between operation year and ^{14}C dated year, Δdate, versus operation year was briefly discussed. For the omnivores, they found a weak negative correlation (R=-0.54, p=0.0001) between the two variables over the whole year. In the paper they later mention that the negative linear slope is speculatively due to consumption of stored food in the end of the year. The range of the sampling date is only between 1978 and 1979 and the linear regression in that picture has a slope close to -1. This will mean that 10 years later, blood samples taken will have an age deviation at least 10 years.

Since the dating is dependent only on the F^{14}C concentration in the sample (and the uncertainties), it should be sufficient to look for a seasonal oscillation in this data set. A least square approximation for a simple sinus function with a wavelength of one year on the form $f(A, \delta, C) = A\sin(2\pi t + \delta) + C$ was done (see Figure 10). The amplitude of this function was approximated to be A= (5.2 ± 23.3)E-4 which indicated that there is a weak correlation between this type of function and the data set.

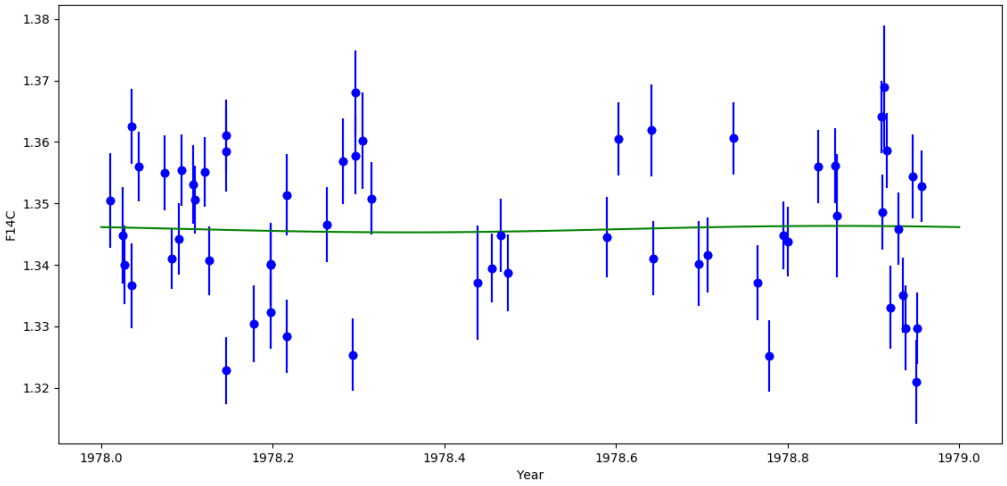

Figure 10: F^{14}C values of the samples from 1978 and a sinus formed regression.

Therefore the carbon concentration in the blood serum samples has weak to no seasonal dependence.

5 Conclusion and Outlook

The aim of this study was to construct a new radiocarbon dating software that considers the human diet, thus increasing the dating accuracy. In absence of other reliable methods to date human tissues (in this case blood serum), it is difficult to confirm which software is more accurate. However, since the time lag between change in ^{14}C concentration in blood serum after consumption of food is very small, a direct comparison between the F^{14}C value of the samples and the calibration curve was made. For samples taken 1978 the accuracy of Caliman was better. However for the samples taken 2005-2014 the model was slightly worse than my reference program. Furthermore, Caliman dated samples approximately to be a year older than my reference program.

The reason the reference program did not produce the same output as Calibomb is that I did not manage to find the most recent updates of how the Calibomb works. Building Caliman on top of Calibomb's software could probably increase the accuracy of the program.

With the aim of the study in mind, stable isotope analysis of δ^{15}N and δ^{13}C could examine the subjects' diet in more detail. Previous studies have exploited this to approximate the amount of fish in the subject's diet. However, it is perhaps possible to determine what kind of plants (C3, C4 or CAM) and meats consumed, thus extracting information about the harvest season for those crops. Additionally, it is possible to determine in more detail which crops are harvested in the country in question, thus weighting the months in the harvest season depending on when specific crops are harvested. However, to reach this accuracy, a more extensive study of the population's diet is required.

Ultimately, to understand how the ^{14}C concentration in humans vary during the year in contrast to the atmosphere's, a long term study could be conducted where test subjects continuously provide small blood samples, which are then analyzed in an AMS, as well as noting their diets.

Acknowledgements

I would like to thank my supervisor Kristina Stenström for helping me understand the radiocarbon subject in good detail. The samples were also gathered by her, which allowed me to reach the conclusions presented in this paper.

References

[1] K Eriksson Stenström, E Andersson Georgiadou, I Gonçalves, G Skog, S Mattsson, C Bertacchi Uvo. Bomb-pulse dating of Swedish and Portuguese atherosclerotic plaque samples - Comparison and possible dietary habits.Paper from PhD thesis *Exploring the Possibilities of* ^{14}*C Bomb-Pulse Dating of Human Tissue Samples*. Lund University, Lund. ISBN 978-91-7623-022-0 (Print)

[2] I Gonçalves, K Stenström, G Skog, S Mattsson, M Nitulescu, J Nilsson. 2010. Dating Components of Human Atherosclerotic Plaques. *Circulation Research* 106:1174-77

[3] E Andersson Georgiadou, I Gonçalves, C Bertacchi Uvo, G Skog, S Mattson, LM Pedro, J Fernandes e Fernandes, K Eriksson Stenström. 2013. Potential influence of diet on bomb-pulse dating of human plaque samples. *Radiocarbon* 55(2):874-84

[4] Queen's University Belfast. <http://calib.org/CALIBomb/> Accessed May 2018

[5] C Bronk Ramsey. 2008. Radiocarbon Dating: Revolutions in Understanding. *Archaeometry* 50(2):249-75

[6] Radiocarbon web-info <http://www.c14dating.com/pret.html> Accessed May 2018

[7] H Godwin. 1962. Half-life of radiocarbon. *Nature* 195:984

[8] Columbia University <http://www.ldeo.columbia.edu/ martins/isohydro/c_14.html> Accessed May 2018

[9] (1996) Known Nuclear Tests Worldwide, 1945–1995. 1996. *Bulletin of the Atomic Scientists* 52(3)61-63, DOI: 10.1080/00963402.1996.11456628

[10] I Levin and B Kromer. 2004. The tropospheric 14CO2 level in mid latitudes of the Northern Hemisphere. *Radiocarbon* 46(3):1261-1272

[11] Q Hua, M Barbetti. 2007. Influence of atmospheric circulation on regional 14CO2 differences. *Journal of Geophysical Research Atmospheres* 112:D19102

[12] M Yim, F Caron. 2006. Life cycle and management of carbon-14 from nuclear power generation. *Progress in Nuclear Energy* 48(1):2-36

[13] IAEA Technical report series, No 421 (2004)

[14] H Oeschger, U Siegenthaler, U Schotterer and A Gugelmann. 1975. A box diffusion model to study the carbon dioxide exchange in nature. *Tellus* 27(2):168-92

[15] ERM Druffel. 1996. Post-bomb radiocarbon records of surface corals from the tropical Atlantic Ocean. *Radiocarbon* 38(3):563–72.

[16] ERM Druffel, S Griffin. 1995. Regional variability of surface ocean radiocarbon from southern Great Barrier Reef corals. *Radiocarbon* 37(2):517–24.

[17] J M Kalish, R Nydal, K H Nedreaas, G S Burr, G L Eine. 2016. A Time History of Pre- and Post-Bomb Radiocarbon in the Barents Sea Derived from Arcto-Norwegian Cod Otoliths. *Radiocarbon* 43(2b):843-55

[18] ICRP. Metabolic data for carbon. 1981. *Annals of the ICRP*. 6(2-3):4-9

[19] LL Tieszen, TW Boutton, KG Tesdahl, NA Slade. 1983. Fractionation and turnover of stable carbon isotopes in animal tissues: Implications for δ^{13}C analysis of diet. *Oecologia* 75(1-2):32-7

[20] TC O'Connell. The isotopic relationship between diet and body proteins; implications for the study of diet in archeology. 1996. D. Phil. Thesis. Univerity of Oxford, Oxford.

[21] R Awsiuk and MF Pazdur. 1986. Regional Suess effect in the Upper Silesia urban area. *Radiocarbon* 28(2A):655-60

[22] ILevin, J Schuchard, B Kromer and K 0 Munnich. 1989. The Continental European Suess Effect. *Radiocarbon* 31(3):431-40

[23] C Slater, T Preston and L T Weaver. 2001. Stable isotopes and the international system of units. *Rapid communications in Mass Spectrometry* 15(15):1270-73

[24] C Kendall and EA Caldwell. 1998. Fundamentals of isotope geochemistry. *Isotope tracers in catchment hydrology* pp. 51-86

[25] M Stuiver and H a Polach. 1977. Discussion Reporting of ^{14}C Data. *Radiocarbon* 19(3):355-63

[26] M H. O'Leary. 1981. Carbon Isotope Fractionation in Plants. *Phytochemistry* 20(4):553-67

[27] E Georgiadou, K Eriksson Stenström, C Bertacchi Uvo, P Nilsson, G Skog, S Mattsson. 2013. Bomb-pulse ^{14}C analysis combined with ^{13}C and ^{15}N measurements in blood serum from residents of Malmö, Sweden. *Radiation and Environmental Biophysics* 52(2):175-87

[28] E Nalborczyk, L J Lacroix and R D Hill. 1975. Environmental influences on light and dark CO_2 fixation by *Kalanchoe daigremontiana*. *Canadian Journal of Botany* 53(11): 1132-1138

[29] M Schoeninger, M DeNiro. 1984. Nitrogen and carbon isotopic composition of bone collagen from marine and terrestrial animals. *Geochimica et Cosmochimica Acta* 48(4):625-39

[30] P J Reimer, T A Brown, R W Reimer. 2004. Discussion: Reporting and Calibration of Post-Bomb 14C Data. *Radiocarbon* 46(3):1299-1304

[31] M Stuiver, G W Pearson. 1986. High-Precision Calibration of the Radiocarbon Time Scale AD 1950-500 BC. *Radiocarbon* 28(2b):805-38

[32] M Stuiver, S W.Robinson. 1974. University of Washington Geosecs North Atlantic carbon-14 results. *Earth and Planetary Science Letters* 23:87-90

[33] D D. Harkness and A Walton. 1969. Carbon-14 in the Biosphere and Humans. *Nature* 223:1216-18

[34] D D. Harkness and A Walton. 1972. Further Investigations of the Transfer of Bomb ^{14}C to Man. *Nature* 240:302-3

[35] R Nydal, K Lövseth and O Syrstad. 1971. Bomb ^{14}C in the Human Population. *Nature* 232:418-21

[36] WS Broecker, A Schulert, EA Olson . 1959. Bomb carbon-14 in human beings. *Science* 130(3371):331-2

[37] RP Manger. 2011. A generic biokinetic model for carbon-14. *Radiation Protection Dosimetry* 143(1):42-51.

[38] MG Beckman, WC Hooper, SE Critchley, TL Ortel. 2010. Venous thromboembolism: a public health concern. *American Journal of Preventive Medicine* 38(4): 495-501

[39] J Genberg, K Stenström, M Elfman and M Olsson. 2010. Development of graphitization of μg-sized samples in Lund University. *Radiocarbon* 52(3):1270-6

[40] G Skog. 2007. The single stage AMS machine at Lund University: Status report. *Nuclear Instruments and Methods in Physics Research Section B: Beam Interactions with Materials and Atoms* 259(1):1-6

[41] M Stuiver, G W Pearson. 1986. High Precicison Calibration of the Radiocarbon Time Scale. *Radiocarbon* 28(2b):805-38

[42] S Hammer, I Levin. 2017. Monthly mean atmospheric D14CO2 at Jungfraujoch and Schauinsland from 1986 to 2016

[43] Jordbruksverket. 2017. Sveriges utrikeshandel med jordbruksvaror och livsmedel 2014-2016. <https://webbutiken.jordbruksverket.se/sv/artiklar/ra1720.html>

[44] E Georgiadou, K Stenström. 2010. Bomb-Pulse Dating of Human Material: Modeling the Influence of Diet. *Radiocarbon* 52

Appendix A

Reference program

```
import matplotlib.pyplot as plt
import numpy as np
import statistics as st

#Import sample data
with open("savedata.txt", 'r') as a:
    data = a.readlines()
    opyear=[]
    fcexc=[]
    errorexc=[]
    for lines in data:
        opyear.append(float(lines.split()[2]))
        fcexc.append(float(lines.split()[0]))
        errorexc.append(float(lines.split()[1]))

#Import Levin data
with open("data.txt", 'r') as a:
    data = a.readlines()
    date=[]
    fc=[]
    error=[]
    for lines in data:
        date.append(1950-float(lines.split()[0]))
        fc.append(float(lines.split()[1]))
        error.append(float(lines.split()[2]))
#Linear model between points and an moving average corresponding to half a

def fcfinals(x):
    fc1=[x for x in fc]
    for i in range(len(date)):
        if x==0:
            break
        n=1
        l=1
        d=fc[i]
        while True:
            if (i+l<len(fc) and date[i]-date[i+l]<x):
                d+=fc1[i+l]
                l+=1
                n+=1
            else:
                fc1[i]=d/n
                break
    return list(reversed(fc1[:600]))
def errfinals(x):
    error1=[x for x in error]
```

```
    for i in range(len(date)):
        if x==0:
            break
        n=1
        l=1
        e=error1[i]
        while True:
            if (i+l<len(fc) and date[i]-date[i+l]<x):
                e+=error[i+l]
                l+=1
                n+=1
            else:
                error1[i]=e/n
                break
    return list(reversed(error1[:600]))

datefinal=list(reversed(date[:600]))


#Excludes first 100 points (1974 onwards)

#Runs the program for all data points

def intersection(d1,d2,c1,c2,f,e1,e2,k):
    x1=d1
    x2=d2
    y1=c1
    y2=c2
    y3=f+e1*k
    y4=f+e2*k

    return ((x1*y2-y1*x2)*(x1-x2)-(x1-x2)*(x1*y4-y3*x2))/((x1-x2)*(y3-y4)-(

def errordat(m,s):
    errfinal=errfinals(s)
    errordata=[]
    for i in range(len(datefinal)):
        errordata.append(np.sqrt((errfinal[i])**2+errorexc[m]**2))
    return errordata

def approxerror(m,s):
    fcfinal=fcfinals(s)
    errordata=errordat(m,s)
    bounds=[] #List of all the  bounds for one sigma
    for i in range(len(datefinal)-1):
        if (fcfinal[i]-errordata[i]<fcexc[m]<fcfinal[i+1]-errordata[i+1]
        or fcfinal[i]-errordata[i]>fcexc[m]>fcfinal[i+1]-errordata[i+1]):
            bounds.append(intersection(datefinal[i],datefinal[i+1],fcfinal[
            , fcfinal[i+1], fcexc[m], errordata[i], errordata[i+1],1))
```

```
        if (fcfinal[i]+errordata[i]<fcexc[m]<fcfinal[i+1]+errordata[i+1]
        or fcfinal[i]+errordata[i]>fcexc[m]>fcfinal[i+1]+errordata[i+1]):
            bounds.append(intersection(datefinal[i],datefinal[i+1],fcfinal[
            , fcfinal[i+1], fcexc[m], errordata[i], errordata[i+1],-1))
    return bounds
    #Intersection of 4 points FIX
    #Returns normalized gaussian
def gaussian(m,s):
    x=fcfinals(s)
    sigma=errorexc[m]
    c=fcexc[m]
    Gau=[]
    for i in range(len(datefinal)-1):
        Gau.append(1/(sigma*np.sqrt(2*np.pi))*np.exp(-1/2*((x[i]-c)/sigma)*
    return Gau
#Returns array of the absolute probabilities between bounds

def totintegral(m,s):
    totint=0
    gau=gaussian(m,s)
    for i in range(len(datefinal)-1):
        totint+=(gau[i]+gau[i+1])/2*(datefinal[i+1]-datefinal[i])
    return totint

def intervals(m,s):
    totint=0
    totint=totintegral(m,s)
    gau=gaussian(m,s)
    integrals=[]
    bounds=approxerror(m,s)
    for j in range(0,len(bounds),2):
        sums=0
        for i in range(len(datefinal)-1):
            if(bounds[j]<datefinal[i]<bounds[j+1]):
                sums+=(gau[i]+gau[i+1])/2*(datefinal[i+1]-datefinal[i])
        integrals.append(sums)
    probability=[x/totint for x in integrals]
    return probability
```

Caliman

```
import matplotlib.pyplot as plt
import numpy as np
import statistics as st


#Import sample data
with open("savedata.txt", 'r') as a:
    data = a.readlines()
    opyear=[]
```

```
    fcexc=[]
    errorexc=[]
    for lines in data:
        opyear.append(float(lines.split()[2]))
        fcexc.append(float(lines.split()[0]))
        errorexc.append(float(lines.split()[1]))

#Import Levin data
with open("data.txt", 'r') as a:
    data = a.readlines()
    date=[]
    fc=[]
    error=[]
    for lines in data:
        date.append(1950-float(lines.split()[0]))
        fc.append(float(lines.split()[1]))
        error.append(float(lines.split()[2]))



#Uses moving average on values between April and October and sets all else


fcnew=list(reversed(fc))
datenew=list(reversed(date))
errornew=list(reversed(error))

startend=[0.3287, 0.4137, 0.49589, 0.5808, 0.6657, 0.8333] #end points of t
boundary=[startend[0],startend[5]]
k=0
last=int(datenew[0])
datefinal=[x for x in datenew]
fcfinal=[x for x in fcnew]
errorfinal=[x for x in errornew]
for i in range(len(datefinal)):
    T=datefinal[i]%1
    t=(boundary[0]-datefinal[i]%1)/(boundary[0]-boundary[1])
    if (boundary[0]<T<boundary[1] and int(datefinal[i])==last):
        fcfinal[i]=fcfinal[i-k-1]*(1-t)+sum(fcnew[i-k:i+1])/len(fcnew[i-k:i
        errorfinal[i]=errorfinal[i-k-1]*(1-t)+sum(errornew[i-k:i+1])/len(er
        k+=1
    elif((last!=int(datefinal[i]) and ((k!=0) or boundary[0]<T<boundary[1])
        last=int(datenew[i])
        fcfinal[i]=fcfinal[i]
        k=0
    else: #If the date is not between
        fcfinal[i]=fcfinal[i-1]
        errorfinal[i]=errorfinal[i-1]
        last=int(datenew[i])
        k=0
```

```
def fcfinals(x):
    fc1=[x for x in fcfinal]
    for i in range(len(date)):
        if x==0:
            break
        n=1
        l=1
        d=fc1[i]
        while True:
            if (i+l<len(fc) and date[i]-date[i+l]<x):
                d+=fc1[i+l]
                l+=1
                n+=1
            else:
                fc1[i]=d/n
                break
    return fc1[100:]
def errorfinals(x):
    error1=[x for x in errorfinal]
    for i in range(len(date)):
        if x==0:
            break
        n=1
        l=1
        e=error1[i]
        while True:
            if (i+l<len(fc) and date[i]-date[i+l]<x):
                e+=error[i+l]
                l+=1
                n+=1
            else:
                error1[i]=e/n
                break
    return error1[100:]

datefinal=datefinal[100:]


#Intersection of 4 points with two diagonally intersecting lines
def intersection(d1,d2,c1,c2,f,e1,e2,k):
    x1=d1
    x2=d2
    y1=c1
    y2=c2
    y3=f+e1*k
    y4=f+e2*k

    return ((x1*y2-y1*x2)*(x1-x2)-(x1-x2)*(x1*y4-y3*x2))/((x1-x2)*(y3-y4)-(
```

```
def errordat(m,s):
    errorfinal=errorfinals(s)
    errordata=[]
    for i in range(len(datefinal)):
        errordata.append(np.sqrt((errorfinal[i])**2+errorexc[m]**2))
    return errordata

def approxerror(m,s):
    fcfinal=fcfinals(s)
    errordata=errordat(m,s)
    bounds=[] #List of all the  bounds for one sigma
    for i in range(len(datefinal)-1):
        if (fcfinal[i]-errordata[i]<fcexc[m]<fcfinal[i+1]-errordata[i+1]
        or fcfinal[i]-errordata[i]>fcexc[m]>fcfinal[i+1]-errordata[i+1]):
            bounds.append(intersection(datefinal[i],datefinal[i+1],fcfinal[
            , fcfinal[i+1], fcexc[m], errordata[i], errordata[i+1],1))

        if (fcfinal[i]+errordata[i]<fcexc[m]<fcfinal[i+1]+errordata[i+1]
        or fcfinal[i]+errordata[i]>fcexc[m]>fcfinal[i+1]+errordata[i+1]):
            bounds.append(intersection(datefinal[i],datefinal[i+1],fcfinal[
            , fcfinal[i+1], fcexc[m], errordata[i], errordata[i+1],-1))
    return bounds
    #Intersection of 4 points FIX
    #Returns normalized gaussian
def gaussian(m,s):
    x=fcfinals(s)
    sigma=errorexc[m]
    c=fcexc[m]
    Gau=[]
    for i in range(len(datefinal)):
        Gau.append(1/(sigma*np.sqrt(2*np.pi))*np.exp(-1/2*((x[i]-c)/sigma)*
    return Gau
#Returns array of the absolute probabilities between bounds

def totintegral(m,s):
    totint=0
    gau=gaussian(m,s)
    for i in range(len(datefinal)-1):
        totint+=(gau[i]+gau[i+1])/2*(datefinal[i+1]-datefinal[i])
    return totint

def intervals(m,s):
    totint=0
    totint=totintegral(m,s)
    gau=gaussian(m,s)
    integrals=[]
    bounds=approxerror(m,k)
    for j in range(0,len(bounds),2):
        sums=0
        for i in range(len(datefinal)-1):
```

```
            if(bounds[j]<datefinal[i]<bounds[j+1]):
                sums+=(gau[i]+gau[i+1])/2*(datefinal[i+1]-datefinal[i])
        integrals.append(sums)
    probability=[x/totint for x in integrals]
    return probability
```

Tables

Table 10: Comparison between the reference program and Caliman using SE of the (2005-2011) data set. The uncertainties are given in 1 σ.

Subject	Year of surgery	$F^{14}C$ of sample	$F^{14}C$ [Ref]	$F^{14}C$ [Man]	SE [Ref]	SE [Man]
1	2006.91	1.0506(42)	1.0620(20)	1.0647(20)	131E-6	173E-6
2	2006.75	1.0597(41)	1.0627(20)	1.0648(20)	9E-6	17E-6
3	2006.75	1.0652(41)	1.0627(20)	1.0648(20)	6E-6	2E-6
4	2007.41	1.0465(43)	1.0567(20)	1.0636(20)	105E-6	259E-6
5	2005.91	1.0660(63)	1.0603(20)	1.0642(20)	32E-6	3E-6
6	2008.33	1.0562(71)	1.0512(20)	1.0574(20)	25E-6	1E-6
7	2007.33	1.0526(52)	1.0542(20)	1.0634(20)	3E-6	117E-6
8	2011.91	1.044(36)	1.0412(20)	1.0467(20)	8E-6	3E-6
9	2007.33	1.0661(41)	1.0542(20)	1.0634(20)	141E-6	7E-6
10	2006.25	1.0554(72)	1.0583(20)	1.0642(20)	9E-6	77E-6
11	2007.99	1.0533(46)	1.0532(20)	1.0587(20)	0E-6	19E-6
12	2007.66	1.0574(37)	1.0592(20)	1.0608(20)	3E-6	6E-6
13	2008.33	1.0499(55)	1.0512(20)	1.0574(20)	2E-6	56E-6
14	2008.25	1.0593(66)	1.0510(20)	1.0587(20)	69E-6	3E-6
15	2011.8	1.0398(48)	1.0406(20)	1.0467(20)	1E-6	35E-6
16	2012.62	1.0352(46)	1.0401(20)	1.0427(20)	25E-6	42E-6
17	2013.53	1.0375(39)	1.0292(20)	1.0352(20)	67E-6	5E-6
Average					37E-6	49E-6
1 SD					47E-6	72E-6

Table 11: Comparison between the reference program and Caliman using SE of the 1978 data set. The uncertainties are given in 1 σ.

Subject	Year of surgery	$F^{14}C$ of sample	$F^{14}C$ [Ref]	$F^{14}C$ [Man]	SE [Ref]	SE [Man]
18	1978.92	1.3331(68)	1.324(68)	1.335(67)	91E-6	4E-6
19	1978.93	1.3459(59)	1.322(68)	1.335(67)	570E-6	119E-6
20	1978.92	1.3586(61)	1.324(68)	1.335(67)	1168E-6	558E-6
21	1978.93	1.3351(61)	1.321(68)	1.335(67)	196E-6	0E-6
22	1978.94	1.3297(69)	1.321(68)	1.335(67)	83E-6	28E-6
23	1978.95	1.3544(69)	1.319(68)	1.335(67)	1240E-6	377E-6
24	1978.95	1.3297(58)	1.318(68)	1.335(67)	132E-6	28E-6
25	1978.96	1.3528(58)	1.317(68)	1.335(67)	1263E-6	317E-6
26	1978.91	1.3486(61)	1.325(68)	1.335(67)	543E-6	185E-6
27	1978.95	1.3210(68)	1.318(68)	1.335(67)	7E-6	195E-6
28	1978.60	1.3605(60)	1.345(68)	1.341(62)	237E-6	380E-6
29	1978.84	1.3560(59)	1.326(68)	1.335(67)	902E-6	442E-6
30	1978.44	1.3371(93)	1.340(68)	1.341(59)	9E-6	18E-6
31	1978.91	1.3641(59)	1.325(68)	1.335(67)	1499E-6	848E-6
32	1978.86	1.3480(100)	1.329(68)	1.335(67)	362E-6	169E-6
33	1978.91	1.3690(100)	1.325(68)	1.335(67)	1944E-6	1157E-6
34	1978.78	1.3252(58)	1.321(68)	1.336(67)	17E-6	108E-6
35	1978.74	1.3606(59)	1.325(68)	1.337(66)	1285E-6	539E-6
36	1978.79	1.3448(55)	1.320(68)	1.335(67)	601E-6	96E-6
37	1978.85	1.3561(61)	1.329(68)	1.335(67)	756E-6	446E-6
38	1978.03	1.3400(64)	1.316(66)	1.343(56)	586E-6	11E-6
39	1978.20	1.3401(67)	1.321(68)	1.343(56)	370E-6	10E-6
40	1978.20	1.3400(65)	1.321(68)	1.343(56)	366E-6	11E-6
41	1978.20	1.3323(60)	1.321(68)	1.343(56)	130E-6	121E-6
42	1978.18	1.3304(62)	1.319(68)	1.343(56)	132E-6	167E-6
43	1978.22	1.3284(60)	1.323(68)	1.343(56)	34E-6	222E-6
44	1978.30	1.3681(68)	1.328(68)	1.343(56)	1623E-6	618E-6
45	1978.30	1.3578(63)	1.328(68)	1.343(56)	899E-6	212E-6
46	1978.30	1.3602(78)	1.328(68)	1.343(56)	1059E-6	293E-6
47	1978.32	1.3508(59)	1.327(68)	1.343(56)	545E-6	63E-6
48	1978.04	1.3560(57)	1.316(68)	1.343(56)	1582E-6	161E-6
49	1978.11	1.3506(55)	1.314(68)	1.343(56)	1338E-6	53E-6
50	1978.15	1.3585(66)	1.316(68)	1.343(56)	1844E-6	231E-6
51	1978.15	1.3611(58)	1.316(68)	1.343(56)	2074E-6	316E-6
52	1978.15	1.3228(54)	1.316(68)	1.343(56)	52E-6	421E-6
53	1978.22	1.3514(66)	1.323(68)	1.343(56)	831E-6	65E-6
54	1978.26	1.3466(61)	1.326(68)	1.343(56)	430E-6	11E-6
55	1978.29	1.3254(59)	1.328(68)	1.343(56)	6E-6	320E-6
56	1978.08	1.3410(49)	1.315(68)	1.343(56)	679E-6	5E-6
57	1978.12	1.3551(57)	1.314(68)	1.343(56)	1718E-6	139E-6
58	1978.28	1.3569(70)	1.327(68)	1.343(56)	880E-6	185E-6
59	1978.47	1.3448(60)	1.344(68)	1.341(59)	0E-6	13E-6
60	1978.64	1.3411(60)	1.342(68)	1.341(63)	1E-6	0E-6
61	1978.59	1.3445(65)	1.344(68)	1.341(62)	0E-6	13E-6
62	1978.71	1.3416(61)	1.328(68)	1.339(65)	195E-6	9E-6

63	1978.47	1.3387(63)	1.344(68)	1.341(59)	26E-6	6E-6
64	1978.64	1.3619(75)	1.343(68)	1.341(63)	359E-6	452E-6
65	1978.80	1.3438(57)	1.321(68)	1.335(67)	518E-6	78E-6
66	1978.70	1.3402(69)	1.330(68)	1.339(65)	100E-6	1E-6
67	1978.76	1.3371(61)	1.322(68)	1.336(66)	218E-6	1E-6
68	1978.01	1.3505(77)	1.315(63)	1.343(56)	1246E-6	52E-6
69	1978.02	1.3448(79)	1.316(65)	1.343(56)	847E-6	2E-6
70	1978.04	1.3366(69)	1.316(67)	1.343(56)	421E-6	45E-6
71	1978.04	1.3626(61)	1.316(67)	1.343(56)	2164E-6	372E-6
72	1978.07	1.3550(61)	1.315(68)	1.343(56)	1583E-6	137E-6
73	1978.09	1.3442(58)	1.315(68)	1.343(56)	872E-6	1E-6
74	1978.09	1.3554(58)	1.315(68)	1.343(56)	1667E-6	146E-6
75	1978.11	1.3531(64)	1.314(68)	1.343(56)	1520E-6	96E-6
76	1978.13	1.3407(56)	1.314(68)	1.343(56)	734E-6	7E-6
77	1978.45	1.3395(56)	1.344(68)	1.341(59)	18E-6	3E-6
Average					710E-6	185E-6
1 SD					634E-6	228E-6

Table 12: Average age comparison for the (2005-2011) data set between the reference program (ΔT_R) and Caliman (ΔT_C) . The uncertainties are given in 1 σ.

Subject	Dated year [Ref]	Dated year [Man]	ΔT_R	ΔT_C
1	2008.90±2.80	2010.24±1.53	1.99±2.80	3.33±1.53
2	2006.90±2.73	2007.25±1.47	0.15±2.73	0.50±1.47
3	2005.41±2.30	2006.17±1.40	-1.34±2.30	-0.58±1.40
4	2009.98±1.79	2011.55±1.06	2.57±1.79	4.14±1.06
5	2005.39±2.34	2006.13±1.59	-0.52±2.34	0.22±1.59
6	2007.51±3.31	2009.05±1.74	-0.82±3.31	0.72±1.74
7	2008.38±3.28	2009.74±1.97	1.05±3.28	2.41±1.97
8	2010.78±1.87	2012.07±0.67	-1.13±1.87	0.16±0.67
9	2005.08±1.99	2006.10±1.40	-2.25±1.99	-1.23±1.40
10	2008.33±3.28	2009.41±2.02	2.08±3.28	3.16±2.02
11	2008.34±3.24	2009.56±1.80	0.35±3.24	1.57±1.80
12	2007.36±2.30	2008.91±1.42	-0.30±2.30	1.25±1.42
13	2008.91±2.82	2010.54±1.90	0.58±2.82	2.21±1.90
14	2006.89±2.78	2008.04±2.37	-1.36±2.78	-0.21±2.37
15	2010.98±1.87	2012.97±0.60	-0.82±1.87	1.17±0.60
16	2011.90±1.86	2013.58±0.85	-0.72±1.86	0.96±0.85
17	2011.47±1.45	2013.14±0.53	-2.06±1.45	-0.39±0.53
Average			-0.150	1.14
1 Sd			1.43	1.5

Table 13: Average age comparison for the 1978 data set between the reference program (ΔT_R) and Caliman (ΔT_C). The uncertainties are given in 1 σ.

Subject	Dated year [Ref]	Dated year [Man]	ΔT_R (yr)	ΔT_C (yr)
18	1977.90±1.02	1977.11±0.47	-1.02±1.02	-1.81±0.47
19	1977.45±1.22	1978.64±0.85	-1.48±1.22	-0.30±0.85
20	1976.43±0.43	1979.13±0.44	-2.49±0.43	0.20±0.44
21	1977.67±1.24	1977.20±0.51	-1.26±1.24	-1.75±0.51
22	1977.93±1.01	1979.14±0.42	-1.01±1.01	0.19±0.42
23	1977.35±1.29	1977.25±0.49	-1.60±1.29	-1.71±0.49
24	1977.93±1.01	1978.03±0.64	-1.02±1.01	-0.88±0.64
25	1977.38±1.26	1979.56±0.14	-1.57±1.26	0.61±0.14
26	1977.43±1.22	1977.07±0.46	-1.48±1.22	-1.53±0.46
27	1978.65±0.75	1977.15±0.48	-0.30±0.75	-1.68±0.48
28	1976.42±0.43	1978.55±0.94	-2.18±0.43	0.12±0.94
29	1976.45±0.42	1977.00±0.45	-2.39±0.42	-1.90±0.45
30	1977.58±1.33	1977.78±0.99	-0.86±1.33	-1.08±0.99
31	1975.88±0.95	1976.90±0.50	-3.03±0.95	-2.02±0.50
32	1977.42±1.25	1979.49±0.14	-1.44±1.25	0.71±0.14
33	1975.87±0.96	1977.07±0.46	-3.05±0.96	-1.67±0.46
34	1978.19±1.19	1978.14±0.63	-0.59±1.19	-0.66±0.63
35	1976.42±0.43	1977.15±0.48	-2.32±0.43	-1.70±0.48
36	1977.45±1.22	1978.51±0.90	-1.34±1.22	0.48±0.90
37	1976.44±0.42	1978.51±0.91	-2.41±0.42	0.31±0.91
38	1977.57±1.31	1978.51±0.91	-0.46±1.31	0.31±0.91
39	1977.57±1.31	1979.03±0.50	-0.63±1.31	0.83±0.50
40	1977.57±1.31	1979.12±0.44	-0.63±1.31	0.94±0.44
41	1977.91±1.01	1979.16±0.42	-0.29±1.01	0.94±0.42
42	1977.92±1.01	1976.88±0.45	-0.26±1.01	-1.41±0.45
43	1977.93±1.01	1977.12±0.48	-0.28±1.01	-1.18±0.48
44	1975.87±0.95	1977.08±0.49	-2.43±0.95	-1.22±0.49
45	1976.43±0.42	1977.56±0.77	-1.86±0.42	-0.75±0.77
46	1976.42±0.43	1977.15±0.48	-1.88±0.43	-0.89±0.48
47	1977.41±1.24	1977.81±0.51	-0.91±1.24	-0.30±0.51
48	1976.45±0.41	1977.11±0.48	-1.60±0.41	-1.04±0.48
49	1977.41±1.23	1977.06±0.46	-0.70±1.23	-1.09±0.46
50	1976.43±0.43	1979.54±0.13	-1.71±0.43	1.39±0.13
51	1976.42±0.43	1977.55±0.78	-1.73±0.43	-0.67±0.78
52	1978.21±1.18	1978.09±0.64	0.07±1.18	-0.17±0.64
53	1977.40±1.25	1979.48±0.15	-0.82±1.25	1.18±0.15
54	1977.45±1.22	1978.50±0.89	-0.82±1.22	0.41±0.89
55	1978.19±1.19	1977.18±0.48	-0.11±1.19	-0.95±0.48
56	1977.47±1.22	1977.14±0.49	-0.61±1.22	-1.14±0.49
57	1977.34±1.28	1978.14±0.64	-0.78±1.28	-0.33±0.64
58	1976.44±0.43	1978.49±0.90	-1.84±0.43	-0.15±0.90
59	1977.45±1.22	1978.14±0.65	-1.01±1.22	-0.45±0.65
60	1977.47±1.22	1978.48±0.91	-1.17±1.22	-0.23±0.91

61	1977.45±1.22	1978.54±0.89	-1.13±1.22	0.06±0.89
62	1977.47±1.22	1977.05±0.48	-1.24±1.22	-1.59±0.48
63	1977.57±1.31	1978.16±0.63	-0.90±1.31	-0.64±0.63
64	1975.89±0.96	1978.50±0.91	-2.75±0.96	-0.19±0.91
65	1977.46±1.22	1978.58±0.87	-1.34±1.22	-0.18±0.87
66	1977.57±1.31	1977.71±0.94	-1.13±1.31	-0.30±0.94
67	1977.58±1.31	1978.39±0.93	-1.18±1.31	0.37±0.93
68	1977.40±1.25	1978.59±0.88	-0.61±1.25	0.55±0.88
69	1977.45±1.22	1977.03±0.46	-0.57±1.22	-1.00±0.46
70	1977.58±1.32	1977.18±0.49	-0.45±1.32	-0.90±0.49
71	1975.89±0.95	1978.15±0.63	-2.15±0.95	0.06±0.63
72	1977.34±1.29	1977.17±0.49	-0.73±1.29	-0.93±0.49
73	1977.46±1.22	1978.15±0.63	-0.63±1.22	0.06±0.63
74	1977.34±1.29	1977.17±0.49	-0.76±1.29	-0.93±0.49
75	1977.37±1.27	1977.24±0.50	-0.74±1.27	-0.87±0.50
76	1977.47±1.22	1978.50±0.90	-0.66±1.22	0.37±0.90
77	1977.57±1.31	1978.52±0.89	-0.89±1.31	0.07±0.89
Average			-1.219	-0.465
1 SD			0.745	0.864